Hindawi
Advances in Materials Science and Engineering
Volume 2021, Article ID 5582150, 20 pages
https://doi.org/10.1155/2021/5582150

Research Article

Experimental Investigation of MgAl-NO_2 and MgAl-CO_3 LDHs on Durability of Mortar and Concrete

Zhanguo Li,[1] Huan Du,[1] Zigeng Wang,[1] Caiyun Jin,[2] and Yue Li[1]

[1]*Key Laboratory of Urban Security and Disaster Engineering of Ministry of Education, Beijing Key Laboratory of Earthquake Engineering and Structural Retrofit, Beijing University of Technology, Beijing 100124, China*
[2]*College of Applied Sciences, Beijing University of Technology, Beijing 100124, China*

Correspondence should be addressed to Zigeng Wang; zigengw@bjut.edu.cn

Received 2 February 2021; Accepted 11 May 2021; Published 25 May 2021

Academic Editor: Shengwen Tang

Two kinds of layered double hydroxides (LDHs), MgAl-NO_2 (N-LDH) and MgAl-CO_3 (C-LDH), were incorporated to study the durability of mortar and concrete. The LDH contents of mortar were 1%, 2%, and 4% by mass and the LDH contents of concrete were 0.5%, 1%, 2%, 4%, respectively. The effect of LDHs on sulfate resistance of mortar was studied through dry-wetting cycle test, compressive strength test, and flexural strength test. In addition, the effects of LDHs on pore structure, chloride resistance, carbonation resistance, shrinkage, and creep of concrete were investigated by SEM, mercury injection test, XRD, chloride ion diffusion coefficient test, chloride salt corrosion depth test, carbonation depth test, shrinkage test, and creep test. The results showed that LDHs can improve the ability of resisting ion corrosion, carbonization, shrinkage, and creep, reduce the pore content, and optimize the pore structure of mortar and concrete to some extent. Moreover, 4% LDHs had a better effect on improving the durability of mortar and concrete compared to 0.5%, 1%, and 2% LDHs, and the effect of C-LDH was better than N-LDH.

1. Introduction

Due to the long-term penetration and corrosion, cement in concrete in marine environment and saline soil area reacted with aluminum, sulfate, and calcium to form expansion stress, which caused volume expansion and reduced the mechanical properties and durability of the concrete [1–7]. Therefore, reducing the penetration rate and concentration of corrosive salts in the concrete is conducive to improve the performance of concrete.

Hydrotalcite compounds are a kind of typical anion intercalation materials, also known as layered double hydroxides (LDHs), which have the characteristics of interlayer anion exchange, thermal stability, memory effect, acidity, and basicity [8, 9] and have been widely applied in many fields, such as catalyst [10], adsorbent [11, 12], drug storage and sustained-release agents [13–15], intercalated optical materials [16], and pollution treatment [17, 18]. For example, in the aspect of concrete admixtures, the polycarboxylate group was inserted into the interlayer of LDHs to slowly release the effect of water reducing agent, which can extend the water reducing effect time and improve the slump operation time of concrete [19, 20].

The interlayer anion exchange property of LDHs was the most important practical property, namely, different anions can enter the interlayer structure of LDHs through exchange behavior, causing the change of the charge density of the laminate and the electrostatic interaction between the laminate and the interlayer anions, and finally changing the interlayer spacing, resulting in a new intercalation structure of LDHs [8]. When the charge density and the diameter of the anion were higher and smaller, the anions were more likely to enter the interlayer. On the contrary, the anions were easier to be replaced. The exchange capacity of common anions in LDHs (equal to the stability of the new structure) was in the order of $CO_3^{2-} > SO_4^{2-} > OH^- > F^- > Cl^- > NO_3^-$, that is, the former anions can be substituted with the latter anions [21]. Based on the principle

that the stability of nitro LDHs was better than chlorine LDHs, a small amount of nitro LDHs (usually 1–5% of the mass of cementitious materials) was added into concrete to solidify chloride ions in concrete through ion exchange, the transmission rate of chloride ions in concrete was delayed, and the durability of concrete was improved [22–27]. The research by Qu et al. [28] showed that adding 1% Ca-Al-NO_3 LDHs into concrete can reduce the chloride ion content by 17%–53%. Chen [29] studied the removal mechanism of Ca-Al-NO_3 LDHs on chloride ion in hardened cement paste and found that LDHs can adsorb Cl^- in cement through ion exchange, so as to reduce the concentration of Cl^- in the paste, and the maximum binding amount of the chloride ion can reach 3.38 mg/g. In addition, the types of interlayer anions of LDHs had different inhibitory effects on chloride ion with the order from strong to weak being NO_2-LDH >NO_3-LDH >C_6H_5COO-LDH >CrO_4-LDH [30]. Yang et al. [22, 31, 32] studied the corrosion resistance of p-aminobenzoate LDHs and nitro LDHs on steel bars, and the results showed that the former had higher binding capacity to chloride ions. The crystallinity of LDHs had a great influence on the early strength of cement slurry. When the crystallinity of LDHs was high, it promoted the hydration reaction of C_3A in cement and inhibited the hydration reaction of C_3S, resulting in relatively low early strength [33]. Guan and Zou [34, 35] evaluated the influence of Li-Al LDHs on the early performance of sulphoaluminate cement clinker. The research results explained that LDHs can increase the early hydration rate of sulphoaluminate cement, increase the contents of early hydration products, and improve the compressive strength.

Compared with noncalcined LDHs, the adsorption of anions on calcined LDHs was significantly improved [36–38] because the layered structure of LDHs was destroyed. However, due to the structure memory effect of LDHs, the layered structure of LDHs was restored after encountering CO_3^{2-}, SO_4^{2-}, and Cl^-. In this process, these ions can be adsorbed in the middle of the layered structure and then playing the role of solidifying the harmful ions [39, 40]. When the calcination temperature of LDHs was higher than 252.8°C, then the structural changes occurred [38]. At present, the common calcination temperature is between 450°C and 650°C [38, 41]. Yoon [42] researched the adsorption of chloride in concrete by Mg-Al LDHs (CLDH) calcined at 450°C. The results showed that the chloride ions were adsorbed in the process of structural reconstruction. The measured ion binding capacities of CLDH were 153 mg/g, which were highly equivalent to the theoretical ion binding capacity of Friedel's salt (121 mg/g). Chen [43] investigated the feasibility of the application of CLDH in UHPC. The research results exhibited that the best dosage of CLDH in UHPC was 1%, and the porosity of concrete decreased and the strength increased. The removal efficiency of CLDH was better than that of fly ash and silica fume. In ordinary concrete, with the increase of CLDH content to 3%, the porosity of concrete displayed a downward trend, and the hydration of cement was promoted [44]. The research results of Duan [36] and Duan et al. [41] also showed that the calcined CLDH can refine the pore structure of concrete. The research results of Geng [45] revealed that the influence of reaction temperature on the chloride binding capacity of CLDH was 38°C > 50°C ≈ 20°C > 3°C. When the pH value was higher than 12.5, increasing the pH value would reduce the chloride binding capacity of CLDH.

At present, there is a lack of systematic research on the effect and mechanism of LDHs on the durability of mortar and concrete with different strength grades. Magnesium aluminum carbonate hydrotalcite (C-LDH) is the most common and widely used hydrotalcite in the market at present with relatively low price. Magnesium aluminum nitrate hydrotalcite (N-LDH) is not stable, and the interlayer nitrate ions are easily replaced by other ions, which is usually used as the precursor of ion exchange. Therefore, this paper used two typical LDHs, N-LDH and C-LDH, to study the influence of sulfate attack resistance of mortar. Additionally, the influence of LDHs and their content on chloride ion permeability, carbonation, shrinkage, and creep on different strength grades of concrete (C30 and C50) were explored.

2. Materials and Methods

2.1. Materials

2.1.1. Raw Materials. The main chemical components of Ordinary Portland Cement, fly ash, magnesium aluminum nitrate hydrotalcite (N-LDH), and magnesium aluminum carbonate hydrotalcite (C-LDH, without calcination) used in this study are shown in Table 1. The cement was the P.O 42.5 R cement produced by Hebei Yanxin Building Materials Co., Ltd. The physical properties are displayed in Table 2. The fly ash was level I coal ash from Shijingshan. The stones were 5~25 mm continuous graded gravel with an apparent density of 2650 kg/m^3, a crushing index of 12%, and a mud content of less than 0.3%. The sand was 0.5~2.0 mm ISO standard sand with an apparent density of 2500 kg/m^3, a fineness modulus of 2.3, SiO_2 content of greater than 96%, and a mud content of no more than 0.2%. The superplasticizer was naphthalene series superplasticizer (solid) with water reduction rate of 20%. The mixing water was tap water. The main technical indicators of LDHs are listed in Table 3.

2.1.2. Sample Preparation. The sample of cement mortar test was prepared as follows. The mix ratio of mortar is shown in Table 4. The cement, standard sand, water, and LDHs were mixed evenly to make mortar by a mixer, then poured into a 40 mm × 40 mm × 160 mm rubber sand mold, and demolded after standing for 24 h. The samples were cured for 28 d under standard conditions (temperature 20 ± 2°C, relative humidity ≥ 95%) and then placed in an oven at 80°C for drying 48 h. Finally, the samples were located in a dry-wet circulation machine for the dry-wetting cycle test of sulfate.

The samples of concrete test were prepared based upon the mix ratio shown in Table 5. Before the durability study, we studied the influence of N-LDH and C-LDH on the mechanical properties of concrete. The results showed that when the content of N-LDH and C-LDH in concrete was higher than 4%, the mechanical properties of concrete

Table 1: Main chemical composition of raw materials (%).

Composition	Cement	Fly ash	N-LDH	C-LDH
CaO	56.132	3.26	0.673	2.94
SiO_2	23.056	52.99	0.276	0.593
Al_2O_3	7.62	36.25	41.54	25.1
MgO	4.9	0.62	55.43	58.9
SO_3	3.56	—	0.0254	1.04
Fe_2O_3	2.36	2.74	0.0235	0.034
K_2O	1.1	1.01	—	
TiO_2	0.51	1.32	—	0.097
MnO	0.28	0.028	—	—
CO_2	—	—	—	10.8
Na_2O	0.19	0.27	0.314	—
ZnO	—	—	1.244	0.388

Table 2: Physical properties of cement.

Density (g/cm^3)	Specific surface area (m^2/kg)	Ignition loss (%)	Set time (min)		Compressive strength (MPa)		Flexural strength (MPa)	
			Initial	Final	3d	28 d	3 d	28 d
3.20	373	2.51	81	191	28.5	56.8	6.1	8.8

Table 3: Main technical indexes of LDHs.

Types	Molecular formula	Electron microscopic mean particle size (μm)		Specific surface area (m^2/g)	Whiteness (%)	Heavy metal (in Pb) (w/%)
		D50	D90			
MgAl-CO_3 LDHs	$Mg_4Al_2(OH)_{12}CO_3{\cdot}mH_2O$	≤5	≤10	≥10	≥90	≤0.001
MgAl-NO_3 LDHs	$Mg_2Al(OH)_6NO_3{\cdot}mH_2O$	≤10	≤20		≥80	

decreased greatly. Therefore, the incorporation of both N-LDH and C-LDH adopts the external-adding method with the amount of 0.5%, 1%, 2%, and 4% of the mass of cement. The cementitious materials, sand, stone, water, and LDHs were mixed evenly in proportion and then poured into a 100 mm × 100 mm × 100 mm mold. After 24 h, the samples were demolded and then cured for 28 d in standard conditions (temperature 20 ± 2°C, relative humidity ≥ 95%).

The concrete samples were prepared for chloride ion resistance test by selecting one surface of the cured concrete samples as the exposed surface with the other five surfaces sealed with epoxy resin. The sealed samples were immersed in a water tank containing 3.5% NaCl solution. The exposed surfaces were faced up and the distance to the liquid surface was 5 cm. To prevent water evaporation, the tank was sealed with a plastic sheet.

The concrete samples were prepared for carbonization resistance test as follows. The cured samples were placed in a drying oven at 60°C for 48 h. One surface of the sample was used as the exposed surface, and the other surfaces were sealed with epoxy resin.

The concrete samples were prepared for shrinkage test and creep test as follows. The cementitious materials, sand, stone, water, and LDHs were mixed based upon Table 5 and poured into two types of molds with dimensions of 100 mm × 100 mm × 515 mm (for shrinkage test) and 100 mm × 100 mm × 400 mm (for creep test). The samples were demolded after 24 h and cured for designed ages in standard conditions.

2.2. Experimental Methods

2.2.1. Cement Mortar Strength Test. Four groups of mortar samples, four samples for each group were tested by GB/T 17671-1999 (cement mortar strength test method (ISO method)). The samples were cured to the standard age, and the strength test was carried out on the SANS electronic universal tester.

2.2.2. Chloride Ion Content of Concrete. Four groups of concrete samples were tested, five samples for each group. The total chloride ion content of the samples was determined by CLU-V rapid chloride ion content tester. The instrument electrode was calibrated before the test, and then the chloride ion selective electrode and the saturated calomel electrode were inserted vertically into the solution for 2 min. The data were recorded after the equipment stabilized. The determination result was expressed as the percentage of chloride ion by the mass of the powder sample.

Table 4: Mortar mix ratio (kg).

Number	Cement	Water	Standard sand	N-LDH/C-LDH
Blank sample	450	225	1350	0
MN-1/MC-1				4.5
MN-2/MC-2				9
MN-4/MC-4				18

Note. MN and MC represent cement mortar mixed with N-LDH and C-LDH, respectively. The incorporation of both N-LDH and C-LDH adopts the external-adding method with the amount of 1%, 2%, and 4% of the mass of cement.

Table 5: Concrete mix ratio (kg/m^3).

	Number	Cement	Water	Fly ash	Stone	Sand	N-LDH/C-LDH	Water reducing agent
C30	L-0	265	175	66	1128	752	0	3.25
	CL-0.5/NL-0.5						1.7	
	CL-1/NL-1						3.3	
	CL-2/NL-2						6.6	
	CL-4/NL-4						13.2	
C50	H-0	389	175	98	1203	515	0	7.3
	CH-0.5/NH-0.5						2.4	
	CH-1/NH-1						4.9	
	CH-2/NH-2						9.7	
	CH-4/NH-4						19.5	

Note. L-0 and H-0 are C30 and C50 concrete without LDHs, respectively. CL and NL are C30 concrete with C-LDH and N-LDH, respectively. CH and NH are C50 concrete with C-LDH and N-LDH, respectively.

2.2.3. Microscopic Morphology Analysis (SEM) of Concrete. After the concrete samples were dried, the FEI Quanta200 scanning electron microscope (SEM) produced by FEI Company in the Netherlands was used to observe the microscopic morphology of the samples. The technical parameters of SEM were as follows: acceleration voltage, 200V~30 kV; magnification, 25~200000; resolution, 3.5 nm.

2.2.4. Mercury Injection Test of Concrete. The concrete samples of L-0, NL-2, CL-2, NL-4, CL-4, H-0, NH-2, CH-2, NH-4, and CH-4 were placed in a drying oven 60°C for 24 h. After that, they were crushed to test the pore structure distribution.

2.2.5. Chloride Corrosion Depth Test of Concrete. Chlorine salt long-term immersion method was adopted to study the effect of LDHs on chloride ion penetration resistance of concrete. Four groups of concrete samples were utilized, five in each group. The sealed samples with the exposed surface facing up were immersed in a water tank containing 3.5% NaCl solution for 180 d. The test solution was changed every 15 d to remain the concentration. The test blocks soaked to the standard age were taken out and cleaned with deionized water and placed in a drying oven at 60°C for 48 h. The concrete powder was taken by layers, and the concrete powder sample was screened through a square hole of 0.08 mm and placed in a drying oven at 105°C for 24 h and then sealed for preservation. 2 g powder was placed in 150 mL deionized water and stirred with a glass rod. After the powder precipitated, the upper liquid was tested by the chloride ion content measuring instrument.

2.2.6. Chloride Ion Diffusion Coefficient of Concrete. The rapid chloride ion diffusion coefficient method (RCM method) was used to study the chloride ion permeability resistance of concrete affected by LDHs, carried out in accordance with GB/T 50082-2009 (standard for test methods of long-term performance and durability of ordinary concrete). Four groups of the concrete, five samples in each group, were investigated. After the test was completed, the samples were cleaned and broken, and 0.1 mol/L $AgNO_3$ solution was sprayed on the broken surface. The depth of chloride ion corrosion was measured after 15 min.

2.2.7. Sulfate Dry-Wetting Cycle Test of Mortar. The sulfate dry-wetting cycle test was used to evaluate the sulfate corrosion resistance of mortar within LDHs. Four groups of mortar samples were tested, four samples in each group. All the mortar samples were immersed in 5% Na_2SO_4 solution for 15 h, air-dried for 1 h, temperature-dried for 6 h with 60°C, and cooled down for 2 h. Each dry-wetting cycle was lasting for 24 h. The test solution was changed every 15 d. The number of dry-wet cycles was set to 0, 20, 40, 60, 80, 100, and 120. The appearance change, mass change rate, compressive strength, and flexural strength were used as evaluation indexes of cement mortar sample under set cycle times.

2.2.8. Carbonation Resistance Test of Concrete. According to the carbonation test in GB/T 50082-2009 (standard for test methods of long-term performance and durability of ordinary concrete), four groups of concrete samples, four samples in each group, were evaluated. The sealed test blocks

were placed in the carbonization box for 3 d, 7 d, 14 d, and 28 d. After taken out, the exposed surface of the test block was broken in the pressure testing machine and sprayed on with 1% phenolphthalein alcohol solution. Then, the carbonization depth of concrete was measured after 30 s.

2.2.9. Shrinkage Test of Concrete. According to the shrinkage test in GB/T 50082-2009, ten groups of concrete samples, three samples in each group, were investigated through contact method. The initial length of the concrete samples was considered when the age was 3 h. Then, the deformation readings of the samples were measured at the intervals of 1 d, 3 d, 7 d, 14 d, 28 d, 45 d, 60 d, 90 d, 120 d, 150 d, 180 d, and 360 d. The shrinkage rates of the samples at each age were calculated.

2.2.10. Compression Creep Test of Concrete. According to the compression creep test in GB/T 50082-2009, ten groups of concrete samples, nine samples in each group, were assessed. The samples were loaded, starting from the age of 28 d. Then, the shrinkage rate and creep strains of the samples were measured at the intervals of 1 d, 3 d, 7 d, 14 d, 28 d, 45 d, 60 d, 90 d, 120 d, 150 d, 180 d, and 360 d. The creep coefficient of the samples at each age was calculated by the following equation:

$$\phi_t = \frac{\varepsilon_t}{\varepsilon_0}, \quad (1)$$

where ϕ_t is the creep coefficient with loading time of t (d), ε_t is the creep strain value with loading time of t (d), and ε_0 is the initial strain value with loading time of 0.

3. Results and Discussion

3.1. Chloride Ion Corrosion Resistance of Concrete

3.1.1. RCM Method. The chloride ion diffusion coefficient of concrete indicates the ability to resist the chloride ion permeability. When the chloride ion diffusion coefficient increased, the chloride ion diffused in concrete more easily, meaning the chloride ion permeability resistance of concrete decreased [46]. It can be seen from Figure 1 that for both C30 and C50 concrete, the chloride ion diffusion coefficient of concrete decreased gradually with the increase of LDH content, indicating that the chloride ion permeability resistance of concrete increased. As can be seen from Figure 1(a), for C30 concrete, when the dosages of the two LDHs were the same, the chloride ion diffusion coefficient of concrete mixed with C-LDH was slightly lower than that of concrete mixed with N-LDH, and the chloride ion diffusion coefficient of NL-4 and CL-4 decreased by 26.3% and 30.3%, respectively, compared with L-0, indicating that C-LDH was more effective in resisting the diffusion of chloride ions in concrete. Because the specific surface area of N-LDH was relatively small (<9 m^2/g) [47] and the anion exchange capacity between layers was limited, the NO_3^- between layers was difficult to be completely replaced by Cl^-. As a result, the resistance to chloride ion permeability of N-LDH was relatively weaker. As can be seen from Figure 1(b), the variation trend of C50 concrete with LDHs was basically the same as C30 concrete, and the chloride ion diffusion coefficient decreased with the increase of LDHs. When the content of LDHs was 4%, the chloride ion diffusion coefficient of C50 concrete decreased the most, and the chloride ion diffusion coefficient of NH-4 and CH-4 decreased by 30.2% and 31.5%, respectively, compared with H-0. The test results showed that the incorporation of LDHs can improve the chloride ion permeability resistance of concrete.

3.1.2. Long-Term Immersion Method. RCM method cannot fully reflect the real diffusion process of chloride ions in concrete [48, 49], and it was difficult to describe the solidification behavior of chloride ions in concrete with LDHs. In order to more truly reveal the influence of LDHs on the chloride ion permeability resistance of concrete, this paper used the chloride salt long-term immersion method to achieve this goal. Figure 2 shows the curves of chloride ion content variation (mass percentage of the powder) of all samples tested by chlorine salt long-term immersion method with corrosion depth. As can be seen from the figure, with the increase of chloride salt corrosion depth, the chloride ion content of all samples exhibited a trend of decline. Compared with the control group, the chloride ion concentration in the concrete samples with LDHs was smaller. For C30 concrete, when the dosages of LDHs were 4%, compared with L-0, the chloride ion concentration of NL-4 and CL-4 at 25 mm decreased by 20.6% and 39.1%, respectively. The variation trend of C50 concrete was basically the same as C30 concrete. Compared with H-0, the chloride ion concentration of NH-4 and CH-4 at 25 mm decreased by 36.8% and 55.4%, respectively. The experimental results displayed that the incorporation of LDHs can improve the resistance to chloride ion permeability of concrete and the degree of ion concentration reduction was higher in C50 concrete. Besides, the effect of C-LDH was better than N-LDH.

In order to display the chloride ion permeability depth of different samples more visually, the chloride ion content test results of each powder sample at a distance of 9~11 mm from the exposed surface are depicted in Figure 3. For C30 concrete, with the increase of the content of LDHs, the content of chloride ion at 9~11 mm of each sample generally showed a downward trend. Compared with L-0, the chloride ion concentration of NL-4 and CL-4 decreased the most, reaching up to 50.7% and 57.7%, respectively. For C50 concrete, the chloride ion concentration of NH-4 and CH-4 decreased by 53% and 58.7%, respectively. Therefore, the incorporation of N-LDH and C-LDH reduced the chloride ion concentration in concrete and improved the chloride ion permeability resistance of concrete to a certain extent. Additionally, the chloride ion permeability resistance effect of C-LDH was better than that of N-LDH.

3.1.3. Hydration Products. In order to explore whether the addition of LDHs reacted with chloride ions in concrete, the powders of L-0, NL-2, NL-4, CL-2, and CL-4 samples, which were 9~11 mm away from the exposed surface, were

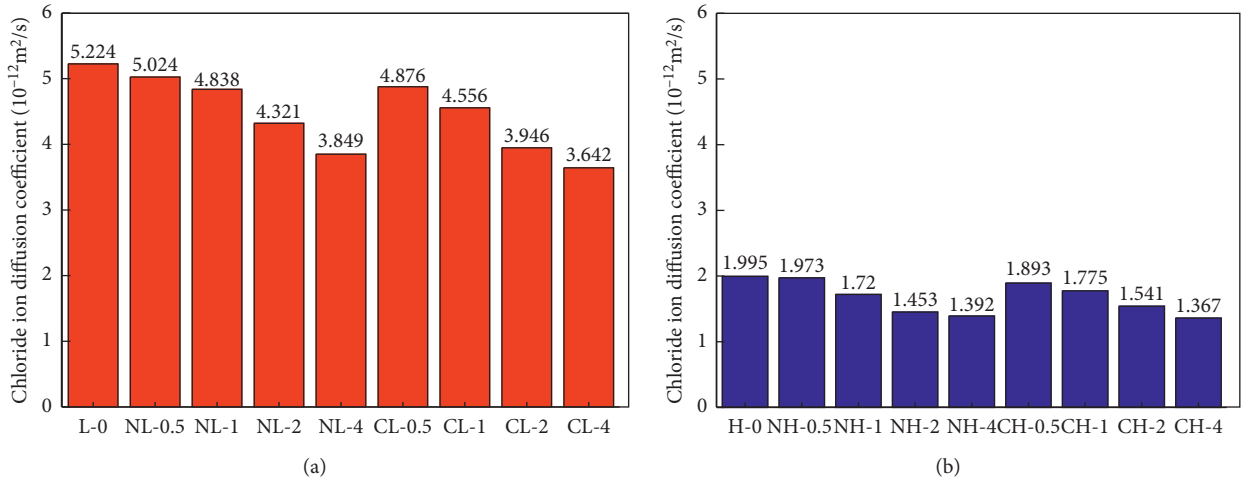

Figure 1: Chloride ion diffusion coefficient of concrete. (a) C30. (b) C50.

analyzed by XRD, as shown in Figure 4. It was found that the main hydration products of each sample after being immersed in chloride solution for 180 d included calcium hydroxide, ettringite, Friedel's salt ($Ca_4Al_2O6{\cdot}10H_2O$), and LDHs. Hence, it was concluded that after intruding into concrete, the chloride ions reacted with cement clinker mineral tricalcium aluminate (C_3A) to form Friedel's salt. Because the structure of Friedel's salt was also a lamellar, the main laminate was composed of calcium aluminum cationic hydroxide ($Ca_2Al(OH)_6^+$) and the interlayer anion was chloride ion. It was difficult to distinguish because the diffraction peak of Friedel's salt overlapped with the peak of LDHs [50, 51]. In order to identify the diffraction peaks of Friedel's salt and LDHs, the XRD patterns of each sample were amplified near $2\theta = 11.24^\circ$, 22.9°, and 60.5°, as shown in Figure 5.

It can be seen from Figure 5 that diffraction peaks of LDHs intercalated with chloride ion appeared in the vicinity of $2\theta = 11.3^\circ$, 22.9°, and 60.5°, respectively, corresponding to (003), (006), and (110) crystal faces of LDHs. (003), (006), and (110) are the unique diffraction peaks of hydrotalcite. The crystal plane diffraction peaks are clear and have no impurity peak, indicating that the material has a high crystallinity and a good layered structure. The Friedel's salt diffraction peaks of L-0 only appeared near $2\theta = 11.3^\circ$ and 22.75°.

Figure 6 shows the XRD comparison of N-LDH and C-LDH before and after chloride ion adsorption. Table 6 shows the layer spacing of each LDH. As can be seen from Figure 6(a), layer spacing did not change much after C-LDH reaction, that is, the structure did not change much. In addition, due to the large specific surface area and strong adsorption of C-LDH, it can be concluded that chloride ions entered the structural layers through the adsorption of C-LDH. Compared with N-LDH, it can be seen from Figure 6(b) that the diffraction peaks corresponding to the (003) and (006) crystal faces of N-LDH after the reaction shifted to a large angle direction, and the lamellar spacing changed from 0.8848 nm before the reaction to 0.7791 nm after the reaction, and the lamellar spacing decreased somewhat. This is because the replacement ability of Cl^- is better than that of NO^{3-}, and the effective radius of Cl^- is smaller than that of NO^{3-}, so the lamellar spacing of N-LDH after the reaction was reduced, which indicated that Cl^- entered the structural layers through the ion exchange of N-LDH.

Therefore, it was believed that N-LDH and C-LDH can absorb chloride ions in concrete environment through interlayer anion exchange and adsorption, respectively, generating magnesium aluminum hydrotalcite intercalated with chloride ion, thus reducing chloride ion concentration in the concrete.

3.2. Pore Structure of Concrete. According to the pore size, the pore structure of concrete can be divided into the following categories: harmless pores (less than 20 nm), less harmful pores (20~100 nm), harmful pores (100~200 nm), and much harmful pores (more than 200 nm). The mercury injection test results of each sample are shown in Figure 7. After processing the data in the figure, the pore contents of different categories and the most available pore sizes distribution of each sample were obtained, as shown in Figure 8. Table 7 shows the values of pore content of each sample.

From Figures 7 and 8 and Table 7, it can be concluded that the total pore volume of L-0 and H-0 was 0.1162 mg/L and 0.0693 mg/L. Compared with L-0, the pore volume of H-0 reduced by 40.4%, indicating that reducing the water-cement ratio can reduce the porosity of concrete. Compared with L-0, the total pore volume of NL-2, CL-2, NL-4, and CL-4 decreased by 3.9%, 8.4%, 10.9%, and 12.7%, respectively. Compared with H-0, the total pore volume of NH-2, CH-2, NH-4, and CH-4 decreased by 9.1%, 18.3%, 23.7%, and 28.4%, respectively. Therefore, it was illustrated that the porosity of concrete decreased with the increase of LDH content in a certain range, and the effect of C-LDH was obviously better than N-LDH.

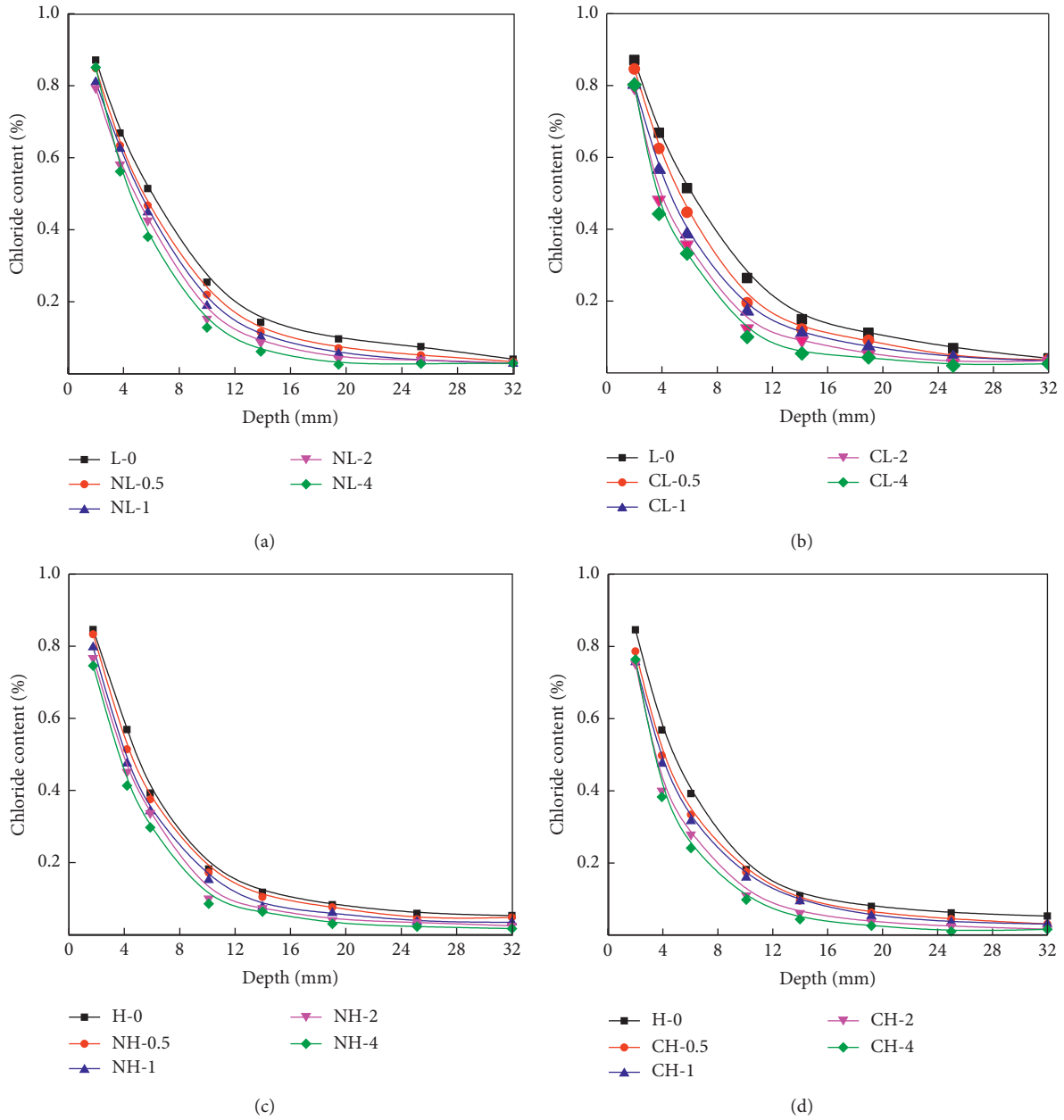

Figure 2: Chloride ion content of concrete. (a) C30 with N-LDH. (b) C30 with C-LDH. (c) C50 with N-LDH. (d) C50 with C-LDH.

Compared with L-0, the harmless pore content of NL-2, CL-2, NL-4, and CL-4 decreased by 1.2%, 2.0%, 5.6%, and 7.5%, respectively. The less harmful pore content decreased by 0.4%, 0.5%, 1.3%, and 1.4%, respectively. The harmful pore content decreased by 14.4%, 33.6%, 43.0%, and 47.9%, respectively, and the much harmful pore content decreased by 24%, 24.2%, 24.7%, and 28.7%, respectively. Compared with H-0, the harmless pore content of NH-2, CH-2, NH-4, and CH-4 decreased by 14.6%, 15.7%, 20.2%, and 22.5%, respectively. The less harmful pore content decreased by 1.1%, 1.8%, 2.6%, and 4.1%, respectively. The harmful pore content decreased by 21.6%, 36.3%, 62.7%, and 76.6%, respectively, and the much harmful pore content decreased by 25.7%, 32.5%, 36.5%, and 42.6%, respectively. The reason was the porosities of L-0 and H-0 which were relatively larger, so LDHs can fill the pores in the concrete to a certain extent and absorb a part of the water in the environment through the interlayer water storage and physical adsorption function. Thus, the water-cement ratio of concrete was reduced and the compactness of concrete increased so that the contents of harmless pore, less harmful pore, harmful pore, and much harmful pore reduced. For C30 concrete, the addition of LDHs made the most probable pore size of concrete shift to the direction of smaller pore size, which indicated that LDHs can optimize the pore structure of C30 concrete and increase the compactness of concrete. For C50 concrete, the effect of LDHs on the most available pore size was relatively small due to its high density.

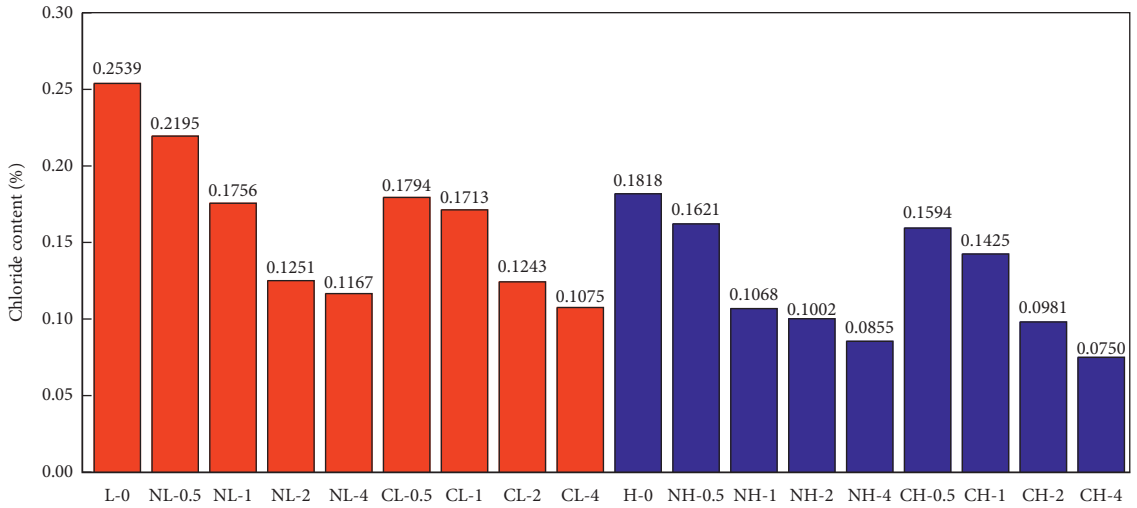

Figure 3: The chloride ion content of concrete 9~11 mm away from the exposed surface of concrete.

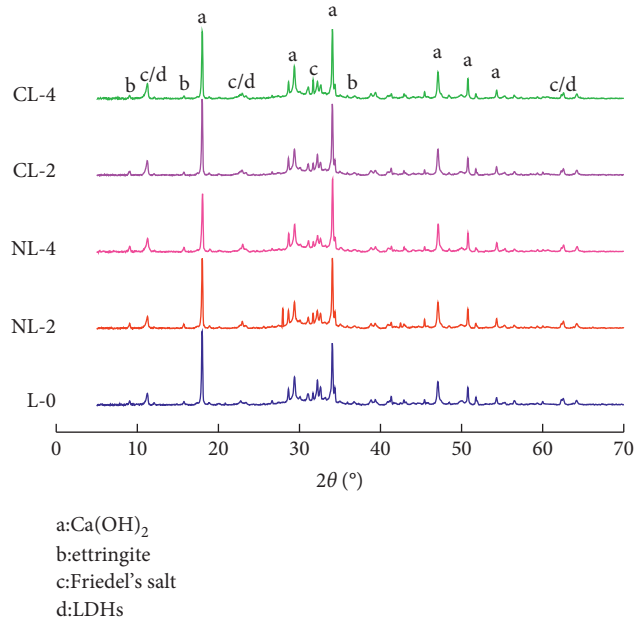

Figure 4: XRD pattern of concrete powder with LDHs at a distance of 9~11 mm from the exposed surface of concrete.

Through the above experimental analysis, it can be revealed that the incorporation of LDHs in a certain range can reduce the content of harmless pores, less harmful pores, harmful pores, and much harmful pores of concrete and improve the pore structure of concrete, and the effect of C-LDH was better than that of N-LDH. Therefore, it was deduced that LDHs can improve the compressive strength and flexural strength of concrete. It should be noted that the C-LDH used in this paper has not been calcined.

3.3. Resistance to Sulfate Attack of Mortar. Figure 9 describes the appearance changes of blank sample, MN-2, MN-4, MC-2, and MC-4 after 0, 40, 80, and 120 cycles of dry-wetting process. As can be seen from the figure, with the increase of the number of cycles, all the samples began to suffer from different degrees of damage. When the dry-wetting cycles were 40 times, the surface of the sample began to become rough and the bare aggregate appeared. When the number of cycles were 80, the surface of each sample began to crack and slightly expand. The edges and corners of the blank sample began to crack and peel off. When the number of cycles reached 120, the blank sample had been corroded very seriously. The surface was loose and some parts fell off. Besides, some white crystals appeared on the surface of the exposed material. For the samples mixed with LDHs, the corrosion phenomenon of MN-4 and MC-4 was relatively lighter, and the surface cracks were few. However, the surface cracks of MN-2 and MC-2 were wide, and the surface and edges of MN-2 peeled off. Therefore, the corrosion of MN-2 and MC-

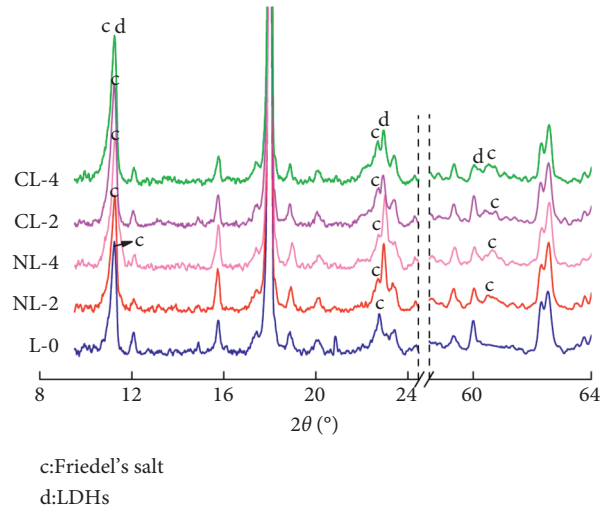

Figure 5: XRD local magnification of concrete with LDHs near 2 $\theta = 11.24^{\circ}$, 22.9°, and 60.5°.

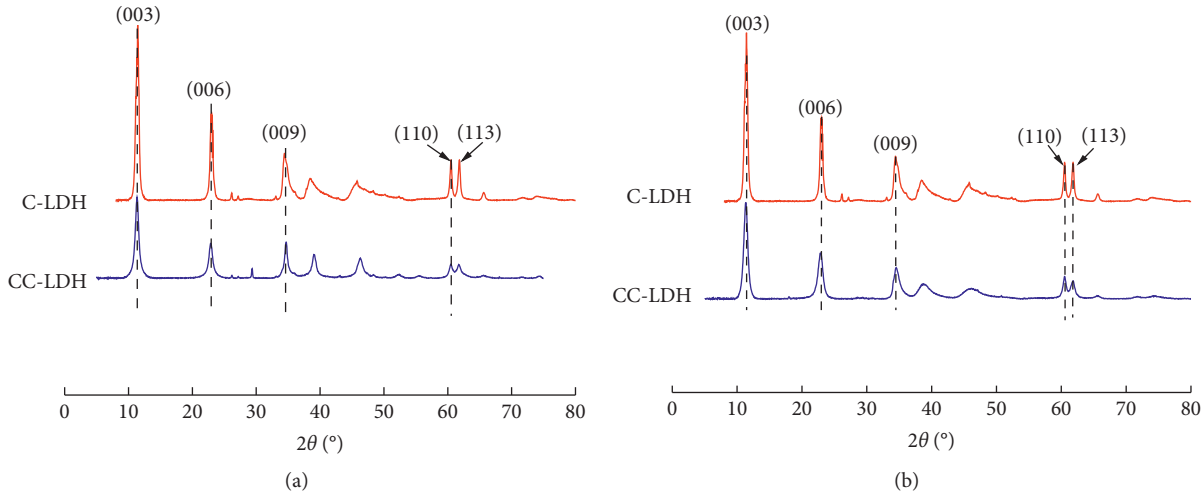

Figure 6: XRD images of (a) C-LDH and (b) N-LDH before and after adsorption of chloride ions.

Table 6: Layer spacing of C-LDH and N-LDH before and after adsorption of chloride ions.

LDHs	C-LDH	N-LDH	CC-LDH	CN-LDH
Layer spacing (nm)	0.7732	0.8848	0.7791	0.7743

Note. CC-LDH represents C-LDH after adsorption of chloride ions; CN-LDH represents N-LDH after adsorption of chloride ions.

2 was more serious than that of MN-4 and MC-4. According to the change of appearance phenomenon, the sulfate corrosion resistance of the five types of the samples was in the order: MC-4 > MN-4 > MC-2 > MN-2 > blank sample.

The mass changes rate of each sample is shown in Figure 10. Some findings were listed. First of all, with the increase of the number of dry-wet cycles, the mass of all samples showed a trend of first increase and then decrease. The mass of blank sample reached the maximum value with the number of cycles of 80, and the mass of blank sample increased by 6.42%. At the 60^{th}, 80^{th}, and 100^{th} cycles, the masses of MN-1, MN-2, and MN-4 increased by 4.87%, 4.95%, and 3.8%; 5.4%, 5.47%, and 4.05%; and 7.11%, 7.15%, and 5.92%, respectively. At the 60^{th}, 80^{th}, and 100^{th} cycles, the masses of MC-1, MC-2, and MC-4 increased by 6.01%, 6.09%, and 4.24%; 6.61%, 6.64%, and 4.89%; and 6.88%, 7.04%, and 5.71%, respectively. It can be seen that the mass of each sample was relatively large when the number of cycles was 80. Secondly, after 120 cycles, the mass of blank sample decreased by 2.54% while the mass of MN-1, MN-2, and MN-4 increased by 0.5%, 1.37%, and 2.71%. In Figure 10(b), the variation pattern of sample mass was

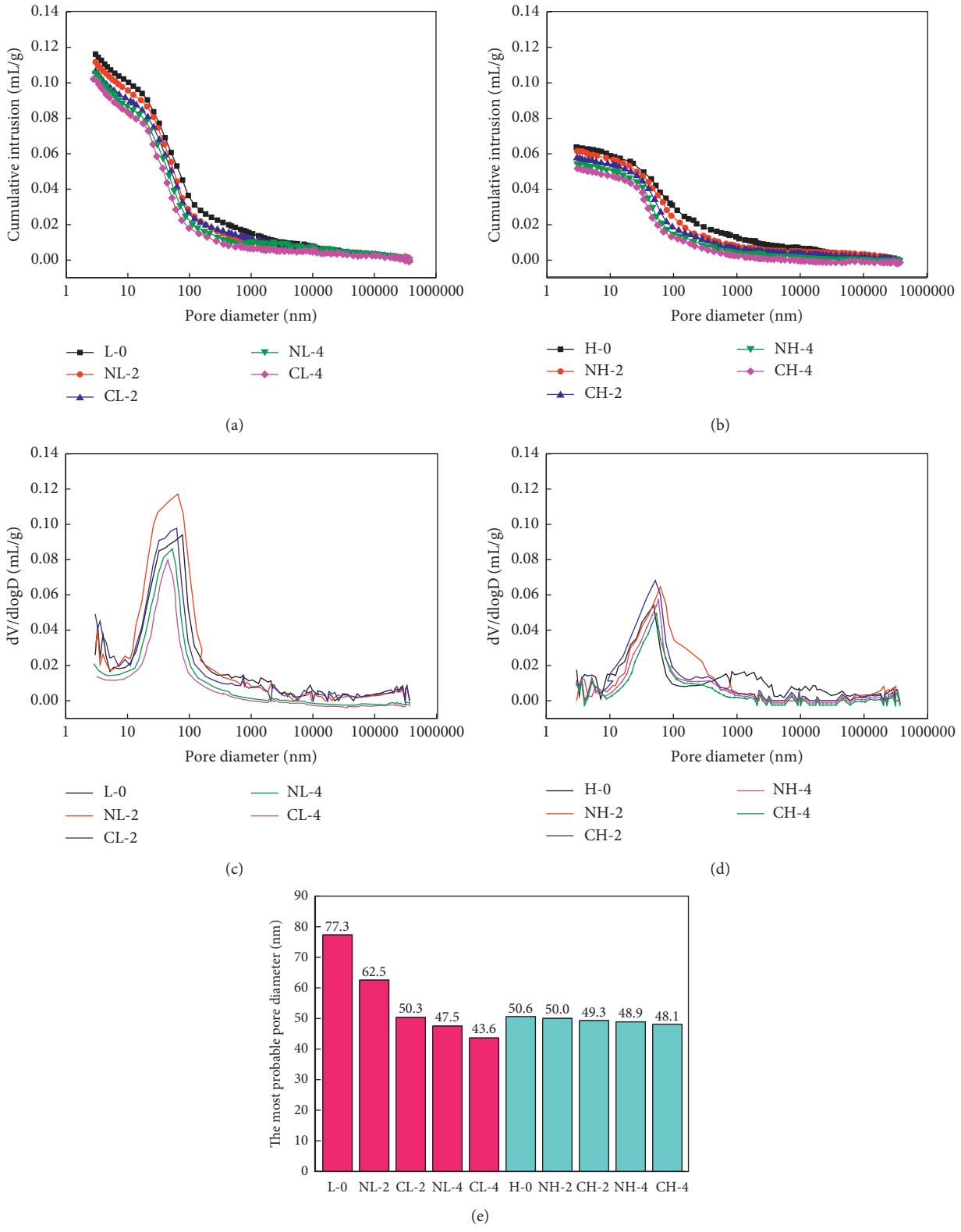

FIGURE 7: Pore size distribution of concrete. Cumulative distribution of pore size of (a) C30 and (b) C50. Differential distribution of pore size of (c) C30 and (d) C50. (e) The most probable pore size of concrete.

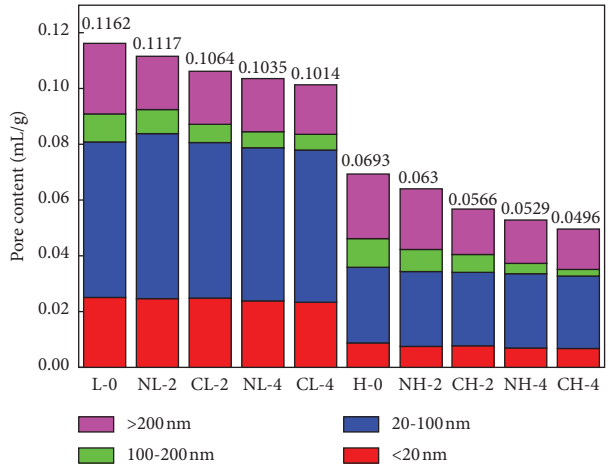

Figure 8: Pore content of concrete.

similar to that in Figure 10(a). After 120 cycles, the masses of MC-1, MC-2, and MC-4 increased by 1.13%, 1.85%, and 3.52%. The mass change rate of each sample was basically consistent with the change pattern of the appearance phenomenon.

At the initial stage of corrosion, the dense structure of mortar had not yet formed. The corrosion products of ettringite and gypsum were generated based on SO_4^{2-} and cement hydration products filled in the pores and cracks in the mortar, increasing the structural compactness and the mass of the sample. With the constant intrusion of SO_4^{2-}, it reacted with hydration products to produce ettringite and gypsum in large quantities. As the volume of these products was about 2.5 times than that of the original hydration products, great internal expansion stress was generated in the material [52]. When the expansion stress exceeded the tensile and shear ultimate strengths of the material, the new cracks were produced, eventually resulting in the sample cracked and the quality declined. In the early stage of the test, N-LDH and C-LDH can prevent SO_4^{2-} intruding into the mortar through interlayer anion exchange and adsorption so that the mass change rate of the sample within LDHs increased compared with the blank sample. With the increase of dry-wetting cycles, the large amount of ettringite and gypsum made the blank samples corrode and peel off constantly and eventually leading to the failure of the sample. The sample with LDHs can react with a part of SO_4^{2-}, thus reducing the generation of expansion products and improving the sulfate corrosion resistance of mortar effectively.

The relationship between the compressive strength of each sample and the number of cycles is displayed in Figure 11. At the beginning of the dry-wetting cycle test, the compressive strengths of all samples increased to some degrees with the increase of the number of cycles, and the compressive strength of the blank sample reached the maximum value of 38.89 MPa when the cycle was 40 times. The compressive strength of the samples with LDHs reached the maximum when the cycle reached 60 times, among which MN-4 and MC-4 had the largest compressive strength, reaching 51.04 MPa and 55.54 MPa, respectively. Compared with the blank sample, the compressive strength of MN-4 and MC-4 increased by 31.2% and 42.8%. This was because the expanding ettringite and gypsum filled the pore structure inside the mortar, which increased the density and strength of mortar. At the later stage of the dry-wetting cycle test, the compressive strength of the samples decreased with the increase of the number of cycles. When the cycle reached 120 times, the compressive strength of the blank sample decreased to 9.37 MPa, and the compressive strengths of the samples with LDHs were significantly higher than the blank sample. The compressive strengths of MN-4 and MC-4 were 25.15 MPa and 32.52 MPa, which were 168.4% and 247.1% higher than the blank sample, respectively. This meant the incorporation of LDHs can react with part of SO_4^{2-}, thus reducing the formation quantity of the expansion products.

Figure 12 displays the variation of the flexural strength of each sample with the number of dry-wetting cycles. It was found that the change rule of the flexural strength was basically consistent with the change rate of mass and the change rule of the compressive strength of the samples. That is to say, the flexural strength of each sample increased first and then decreased with the increase of the number of cycles. The flexural strength of blank sample reached the maximum value of 6.58 MPa when the number of cycles was 40, and then the flexural strength decreased. The flexural strength of MN-4 and MC-4 reached the maximum values at 60 cycles with the values of 8.76 MPa and 9.8 MPa, respectively, increasing by 33.1% and 48.9% compared with the blank sample. When the number of cycles was 120, the flexural strength of the blank sample was 0.99 MPa. In contrast, the flexural strengths of MN-4 and MC-4 were 4.28 MPa and 6.1 MPa, respectively, which increased by 332.3% and 516.2% compared with the blank sample.

According to the strength test results, the compressive strength and flexural strength of mortar samples with the 1% and 2% contents of LDHs were lower than those with 4% content of LDHs after 120 dry-wetting cycles. With the increase of the dosage of LDHs, the porosity of the sample decreased and the pore structure was optimized. Thus, the

Table 7: The 28 d pore content of concrete.

Pore size (nm)	Pore content (mg/L)									
	L-0	NL-2	CL-2	NL-4	CL-4	H-0	NH-2	CH-2	NH-4	CH-4
<20	0.0252	0.0249	0.0247	0.0238	0.02333	0.0089	0.0076	0.0075	0.0071	0.0069
20~100	0.0556	0.0554	0.0553	0.0549	0.0548	0.0271	0.0268	0.0266	0.0264	0.0260
100~200	0.01017	0.00871	0.00675	0.0058	0.0053	0.0102	0.008	0.0065	0.0038	0.0024
>200	0.02524	0.01914	0.01918	0.019000	0.018	0.0231	0.0218	0.016	0.0156	0.0143

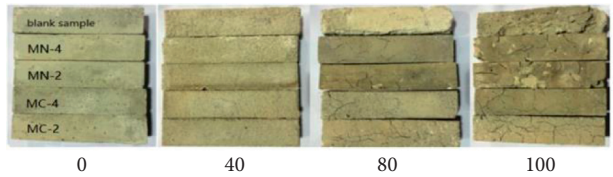

Figure 9: The appearance change of mortar under dry-wetting cycles.

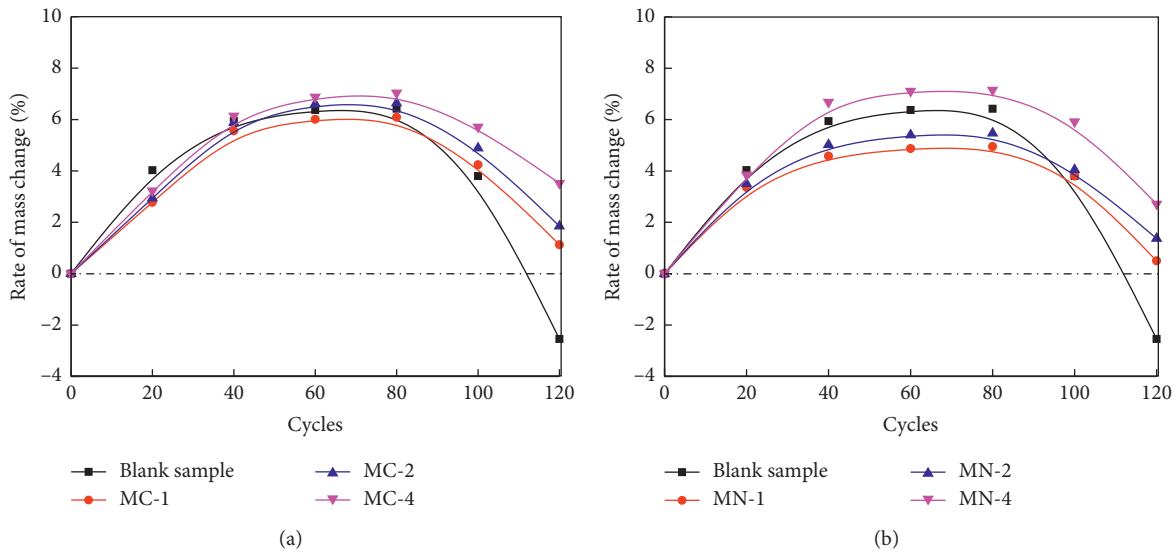

Figure 10: Mass change rate of mortar under dry-wetting cycles. (a) Mortar with N-LDH. (b) Mortar with C-LDH.

strength increased to a certain extent, and the effect of C-LDH was better than that of N-LDH.

3.4. Carbonation Resistance of Concrete. The relationship between concrete carbonation depth and age is shown in Figure 13. Firstly, for each sample, the carbonation depth of concrete increased with the increase of carbonation time. Secondly, at the early stage of carbonation, the carbonation depth of all samples decreased with the increase of the content of LDHs, indicating that the incorporation of LDHs can improve the carbonation resistance of concrete at the early stage. Thirdly, after 28 d of carbonation, the carbonation depth of concrete decreased with the increase of the content of LDHs. For C30 concrete, the carbonation depths of NL-4 and CL-4 were 10.33 mm and 9.62 mm after 28 d, which decreased by 20.1% and 25.6% compared with the blank sample, respectively. For C50 concrete, the carbonation depths of NH-4 and CH-4 were 5.08 mm and 4.73 mm after 28 d, which were 19.1% and 24.7% lower than the blank sample, respectively. Therefore, the incorporation of LDHs reduced the carbonation depth of concrete, and the carbonation resistance of C-LDH was better than that of N-LDH.

Figure 14 shows the carbonation depth values of L-0, CL-2, NL-2, H-0, CH-2, and NH-2 at the carbonation age of 28 d. It can be seen that the carbonation depths of NL-2 and CL-2 at 28 d decreased by 14.8% and 24.3%, respectively, compared with L-0. The carbonation depths of NH-2 and CH-2 at 28 d decreased by 16.1% and 21.7%, respectively, compared with H-0. Therefore, the carbonization resistance of C-LDH was better than that of N-LDH. The reason was

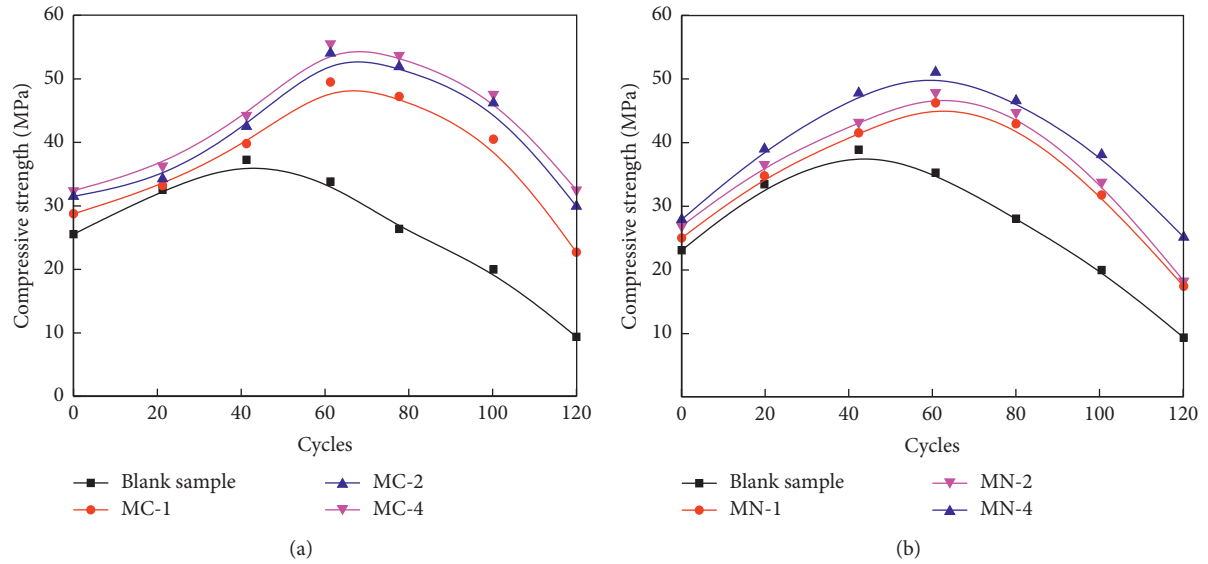

Figure 11: The compressive strength of mortar under dry-wetting cycles. (a) Mortar with N-LDH. (b) Mortar with C-LDH.

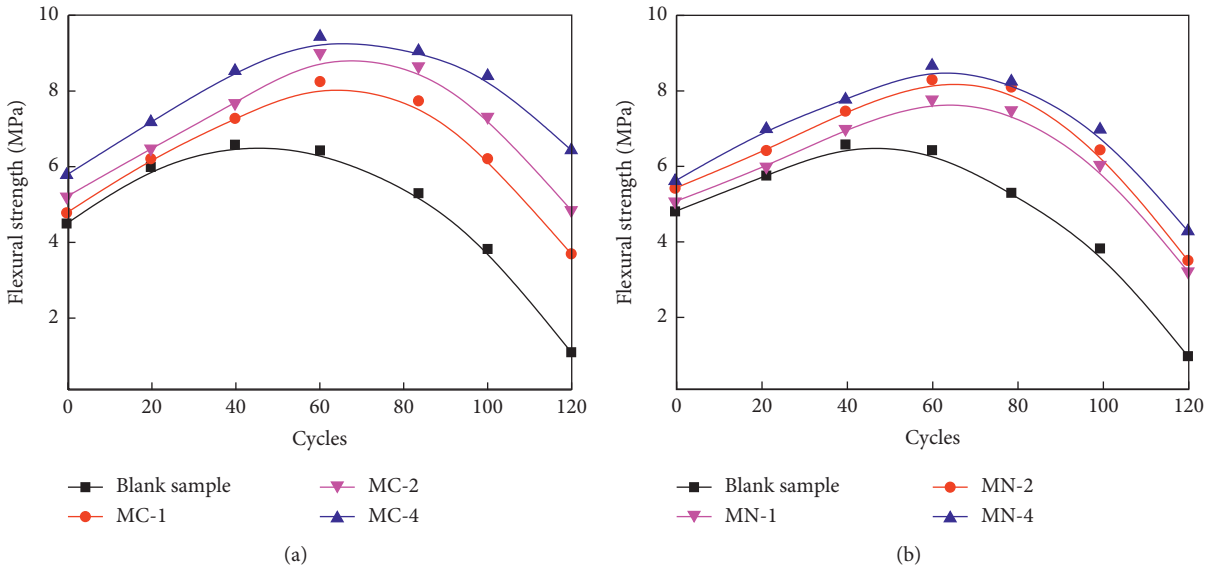

Figure 12: The flexural strength of mortar under dry-wetting cycles. (a) Mortar with N-LDH. (b) Mortar with C-LDH.

that the specific surface area of C-LDH was larger than N-LDH [53] with a stronger interlayer water storage capacity. Thus, the water-cement ratio of concrete was reduced more obviously so that the pore structure was more compacted and the density was smaller.

The carbonization regions of L-0, CL-2, and NL-2 and H-0, CH-2, and NH-2 were sampled for XRD analysis, as shown in Figure 15, after carbonization for 28 d, and Table 8 exhibits the mass fraction of each substance. It can be seen that the main products of each sample after carbonization were calcium carbonate, silica, and dolomite, and $Ca(OH)_2$ had almost been consumed. After adding LDHs into the concrete, the amount of $CaCO_3$ in the carbonization zone was reduced. For example, compared with L-0, the amount of $CaCO_3$ in carbonization zones of NL-2 and CL-2 was reduced by 31.3% and 50.4%, respectively. Compared with H-0, the amount of NH-2 and CH-2 was decreased by 9.9% and 15.3%, respectively.

In order to verify the test results of XRD, the carbonization region of NL-2 and CL-2 was sampled. The micromorphology of the samples was analyzed after drying, as shown in Figure 16. Under SEM, the LDHs were lamellar and attached to the surface of C-S-H gel. Therefore, we can conclude that the concrete mixed with N-LDH and C-LDH absorbed CO_3^{2-} in the concrete environment and generated magnesium aluminum hydrotalcite structure with carbonate intercalation.

According to the conclusion of chloride ion absorption in Section 3.1.3, it can be seen that C-LDH has a strong adsorption effect and N-LDH has a strong ion exchange

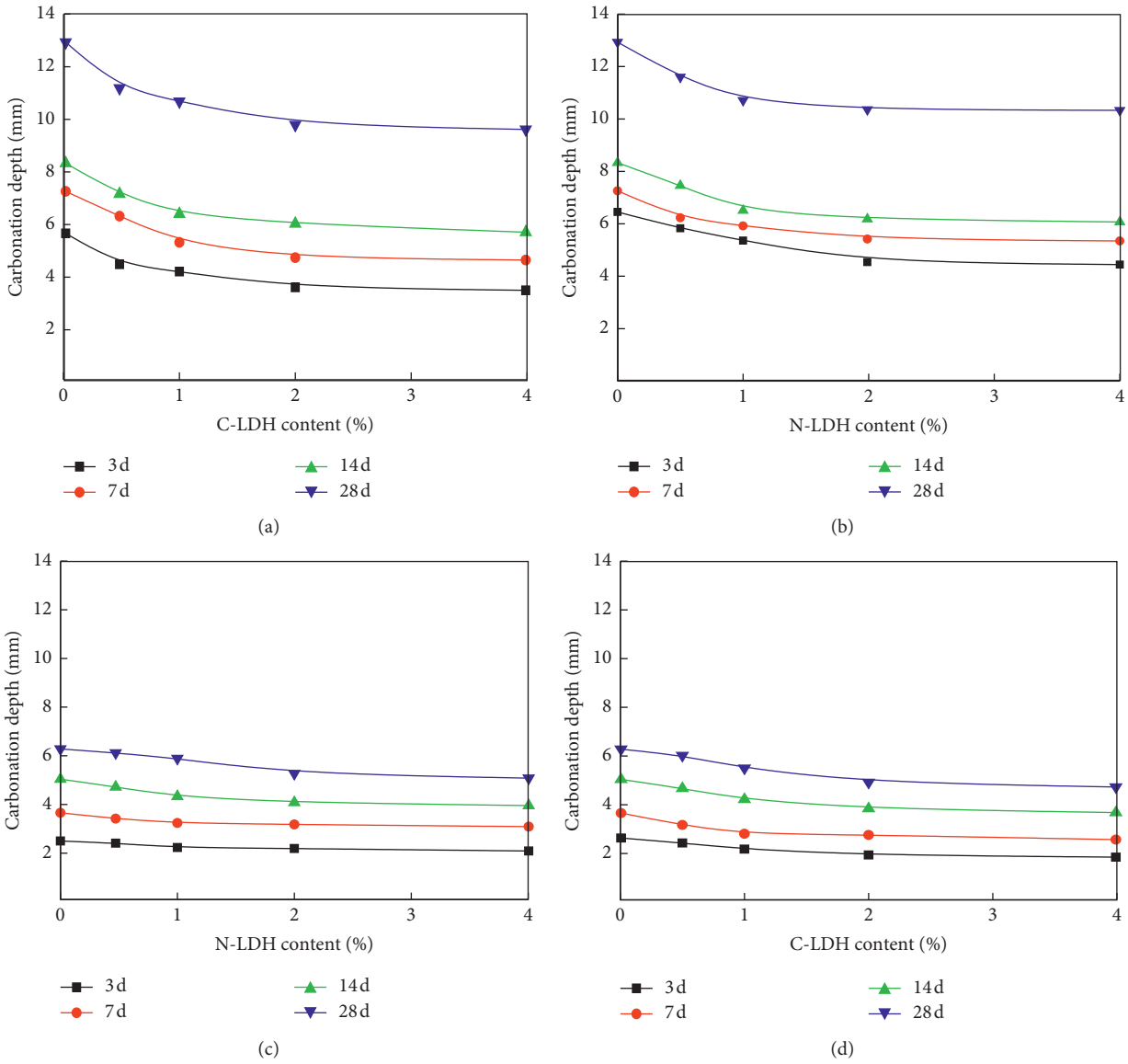

Figure 13: Relationship between carbonation depth of concrete and content of LDHs. (a) C30 with N-LDH. (b) C30 with C-LDH. (c) C50 with N-LDH. (d) C50 with C-LDH.

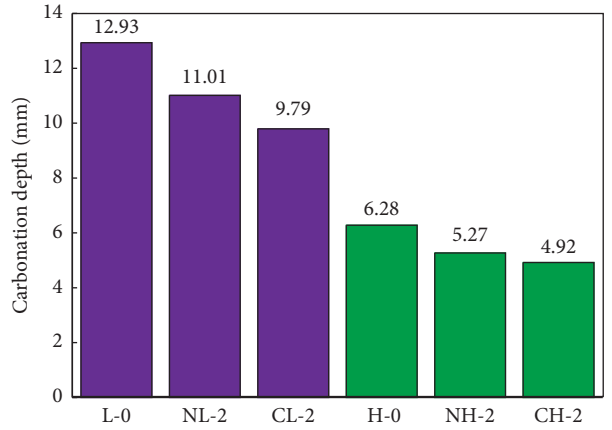

Figure 14: Carbonation depth of concrete with LDHs at 28 d.

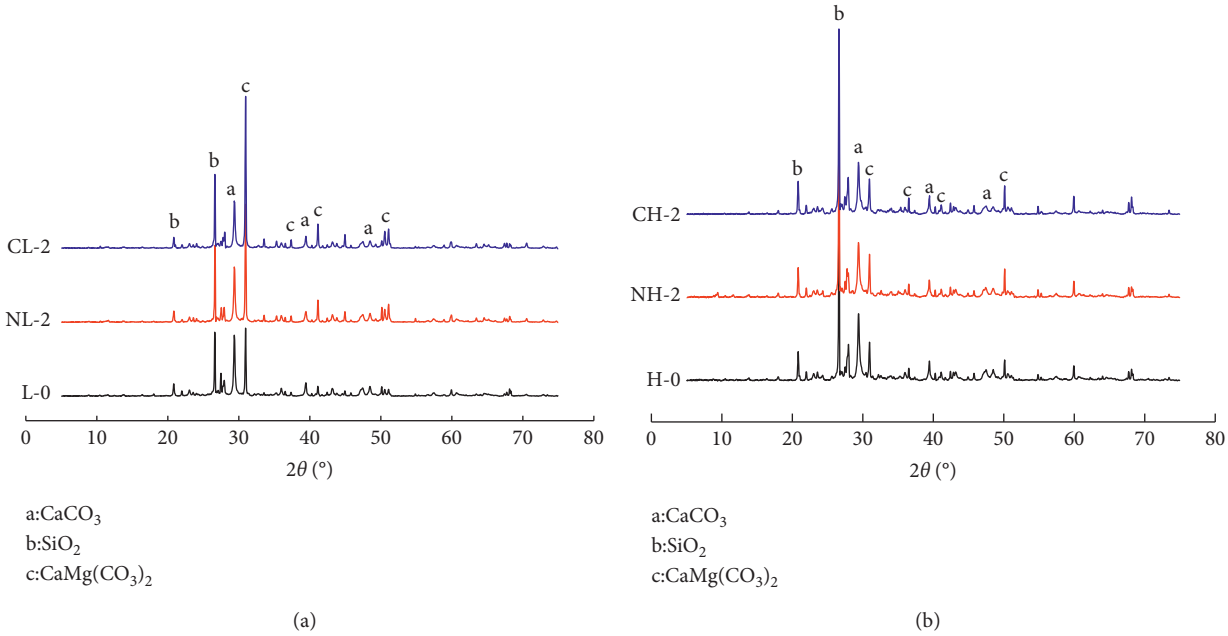

Figure 15: XRD of concrete carbonation zone. (a) L-0, NL-2, and CL-2. (b) H-0, NH-2, and CH-2.

effect. Since both of them have a certain resistance to CO_2, it can be concluded that N-LDH adsorbs CO_3^{2-} through ion exchange, while C-LDH adsorbs CO_3^{2-} through adsorption.

3.5. Shrinkage Performance of Concrete. The experimental results of the influence of the LDHs on the shrinkage performance of concrete are shown in Figure 17. It can be seen that the shrinkage of C30 and C50 concrete with N-LDH and C-LDH at different ages showed a downward trend. With the increase of the amount of LDHs, the shrinkage values of the concrete decreased. When the contents of N-LDH and C-LDH in the concrete were the same, the shrinkage of C50 concrete was lower than that of C30 concrete. In addition, the shrinkage of concrete with C-LDH decreased more, compared with the concrete with N-LDH.

In order to assess the variation of concrete shrinkage after adding N-LDH and C-LDH, the shrinkage test results of C30 and C50 concrete at the age of 28 d were studied, as shown in Figure 18. It was calculated that the shrinkage of NL-2, Cl-2, NL-4, and CL-4 decreased by 5.3%, 8.4%, 15.4%, and 16.3%, respectively, compared with L0. Compared with H0, the shrinkage of NH-2, CH-2, NH-4, and CH-4 decreased by 18.3%, 21.1%, 30.1%, and 33.3%, respectively. By analyzing the above results together with the experimental results in Section 3.2, it can be found that the decreasing trend of shrinkage was consistent with the decreasing trend of total porosity of concrete. Therefore, we believed that the main reason for the decrease of shrinkage rate of concrete after adding N-LDH or C-LDH was that N-LDH or C-LDH absorbed part of the water in the environment through interlayer water storage and physical adsorption function, thus reducing the water-cement ratio of the concrete, increasing the compactness and improving the pore structure of concrete.

3.6. Creep Performance of Concrete. The experimental results of the influence of LDHs on the creep performance of concrete are depicted in Figure 19. It can be seen that when N-LDH and C-LDH were added into C30 or C50, the creep coefficient of concrete displayed a downward trend. The creep coefficient decreased with the contents of N-LDH and C-LDH increased. Compared with N-LDH, the creep coefficient of the concrete with the same content of C-LDH decreased more. Hence, it was concluded that N-LDH and C-LDH both can reduce the creep coefficient of the concrete, and the effect of C-LDH was better than N-LDH.

The creep coefficient test results of C30 and C50 concrete at the age of 28 days are marked in Figure 20. It can be seen that the creep coefficients of NL-2, CL-2, NL-4, and CL-4 decreased by 2.0%, 4.5%, 5.2%, and 7.1%, respectively, compared with L0. Compared with H0, the creep coefficients of NH-2, CH-2, NH-4, and CH-4 decreased by 9.8%, 11.1%, 12.4%, and 18.5%, respectively.

Table 8: Mass fraction of each substance in concrete carbonation zone (%).

Sample	L-0	NL-2	CL-2	H-0	NH-2	CH-2
SiO_2	13.8	12.7	9.1	29	33	34.1
$CaCO_3$	11.5	7.9	5.7	11.1	10	9.4
$CaMg(CO_3)_2$	49.7	67	73.8	24.6	26.4	20.5
$Ca(OH)_2$	0.7	0.2	0.2	1.2	1.2	1.3
Ettringite	16.2	9.1	7.9	22.8	16	23.6
Others	8.1	3.1	3.3	11.3	13.4	11.1

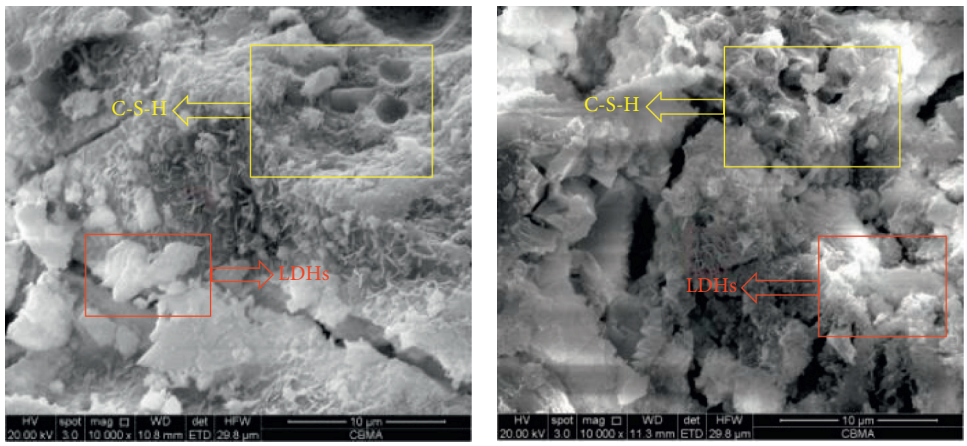

(a) (b)

Figure 16: SEM image of concrete carbonation zone. (a) NL-2. (b) CL-2.

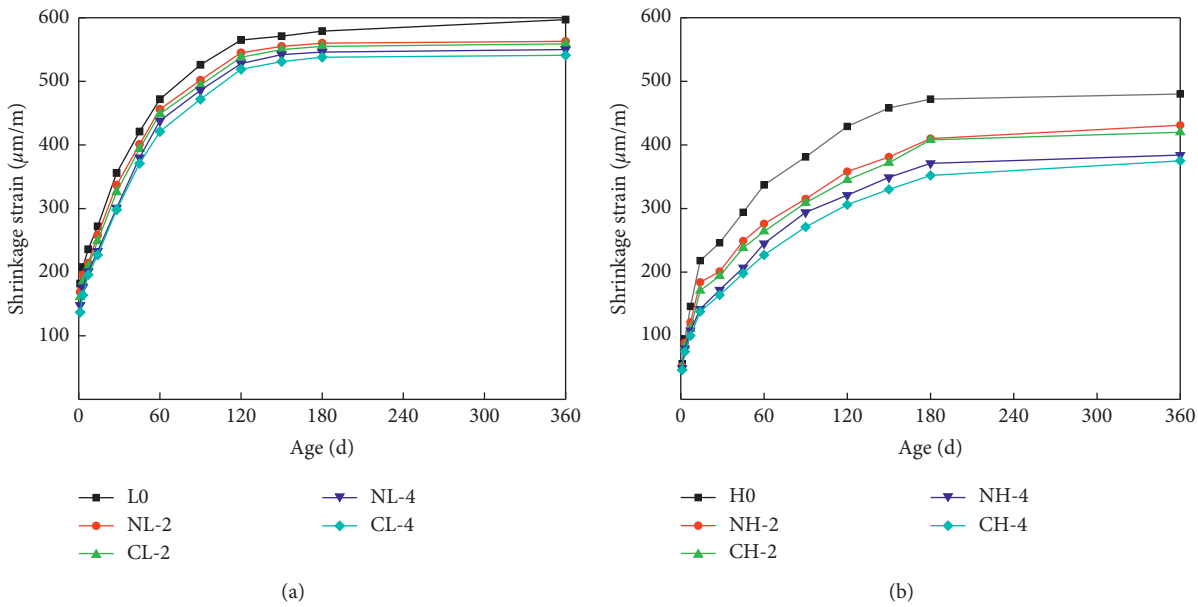

(a) (b)

Figure 17: Shrinkage rate of concrete at different ages. (a) C30. (b) C50.

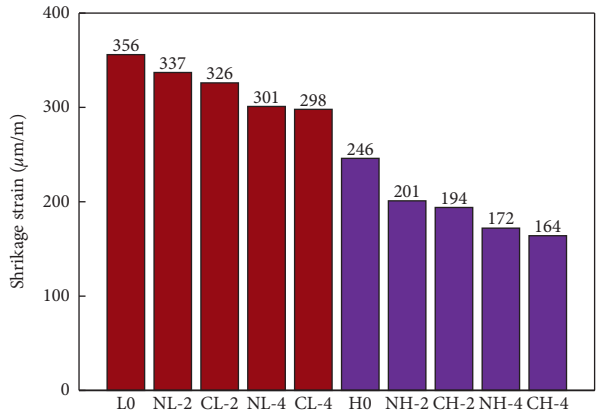

Figure 18: Shrinkage rate of concrete at the age of 28 d.

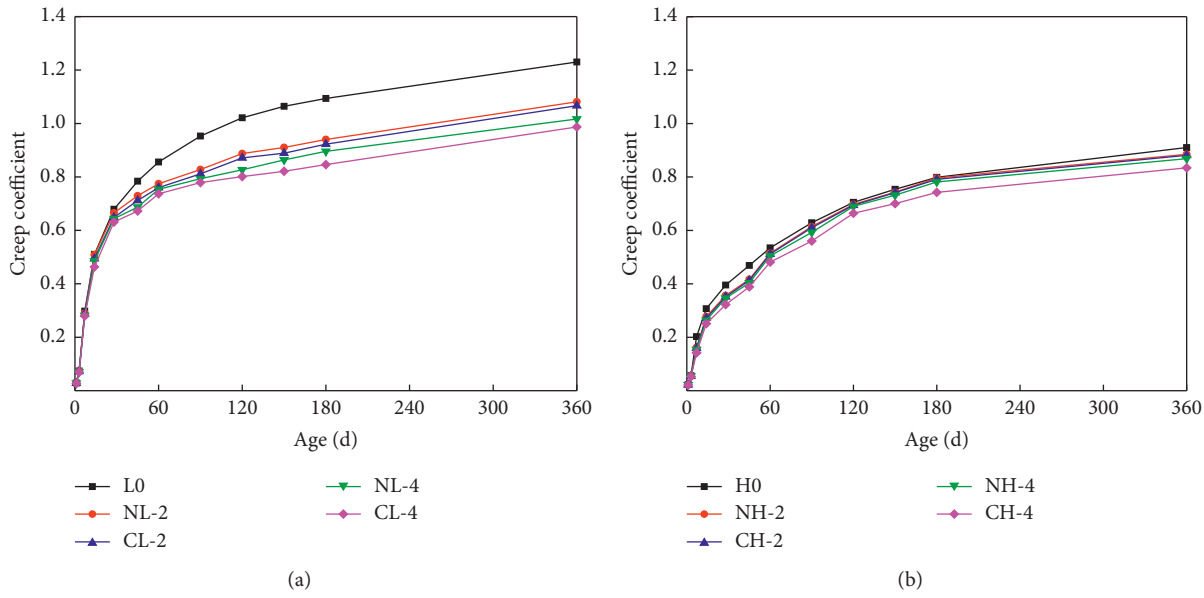

Figure 19: Creep coefficient of concrete at different ages. (a) C30. (b) C50.

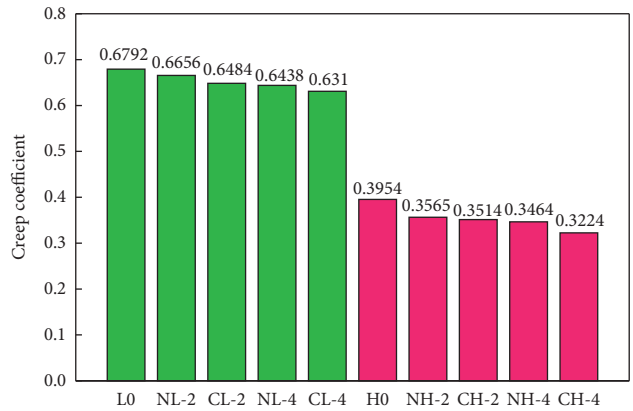

Figure 20: Creep coefficient of concrete at the age of 28 d.

4. Conclusions

In this paper, two typical LDH materials, magnesium aluminum nitrate hydrotalcite (N-LDH) and magnesium aluminum carbonate hydrotalcite (C-LDH), were introduced into mortar and concrete to explore the influence on durability. The maximum content of N-LDH and C-LDH is 4%. It can be seen from this paper that with the gradual increase of N-LDH and C-LDH content, the durability indexes of the studied concrete are improved. Therefore, we speculate that when the content of N-LDH and C-LDH is higher than 4%, the durability index will continue to improve.

When the content of N-LDH and C-LDH is less than 4%, the following conclusions are drawn:

(1) N-LDH and C-LDH can remove chloride ions in solution by anion exchange and adsorption, respectively. The diffusion coefficient of chloride ions in concrete decreased with the increase of the content of LDHs. Both N-LDH and C-LDH can react with chloride ions intruding into concrete and generate magnesium aluminum hydrotalcite intercalated with chloride ions, thus reducing the concentration of chloride ions inside the concrete. C-LDH was better than N-LDH in improving chloride ion permeability resistance of concrete.

(2) The proper amount of LDHs can optimize the pore structure of concrete to a certain extent, and the addition of LDHs can reduce the content of harmless pores, less harmful pores, harmful pores, and much harmful pores of concrete. C-LDH was better than N-LDH in improving concrete pore structure.

(3) The mass change rate, compressive strength, and flexural strength of mortar increased firstly and then decreased with the increase of dry-wetting cycles. N-LDH and C-LDH can adsorb SO_4^{2-} in the environment. With the increase of LDHs, the sulfate corrosion resistance of mortar was improved, and the sulfate corrosion resistance of C-LDH was better than that of N-LDH.

(4) N-LDH and C-LDH can remove CO_3^{2-} in the environment through the interlayer anion exchange and adsorption, respectively, and the adsorption capacity of C-LDH was better than that of N-LDH. At the early stage of carbonization, the carbonation resistance of concrete increased with the increase of LDHs. When the age was 28 d, the carbonation depth of concrete decreased with the increase of LDHs. Both N-LDH and C-LDH can adsorb CO_3^{2-} in concrete environment and produce lamellar magnesium aluminum carbonate hydrotalcite. C-LDH was better than N-LDH in improving the carbonization resistance of concrete.

(5) The shrinkage and creep of concrete can be reduced by adding LDHs into concrete because of the optimization of pore structure, and the effect of C-LDH was better than that of N-LDH.

Data Availability

All the research data have been included in the manuscript and the figures.

Conflicts of Interest

The authors declare that the research was conducted in the absence of any commercial or financial relationships that could be construed as potential conflicts of interest.

Acknowledgments

The authors would like to acknowledge the financial support by the Beijing Municipal Natural Science Foundation (8202005); National Natural Science Foundation of China (51808015); National Natural Science Foundation of China (52078015); and General Project of Science and Technology Plan of Beijing Municipal Commission of Education (KM202110005018).

References

[1] J. Li, Z. Wu, C. Shi, Q. Yuan, and Z. Zhang, "Durability of ultra-high performance concrete - a review," *Construction and Building Materials*, vol. 255, Article ID 119296, 2020.

[2] A. M. Rashad, "An overview on rheology, mechanical properties and durability of high-volume slag used as a cement replacement in paste, mortar and concrete," *Construction and Building Materials*, vol. 187, pp. 89–117, 2018.

[3] S. W. Tang, Y. Yao, C. Andrade, and Z. J. Li, "Recent durability studies on concrete structure," *Cement and Concrete Research*, vol. 78, pp. 143–154, 2015.

[4] Z. Cheng-lin, "Numerical investigation of external sulfate attack and its effect on chloride binding and diffusion in concrete," *Construction and Building Materials*, vol. 282, 2021.

[5] Q. F. Liu, "Prediction of chloride diffusivity in concrete using artificial neural network: modelling and performance evaluation," *Construction and Building Materials*, vol. 268, p. 20, 2021.

[6] L.-x. Mao, Z. Hu, J. Xia et al., "Multi-phase modelling of electrochemical rehabilitation for ASR and chloride affected concrete composites," *Composite Structures*, vol. 207, pp. 176–189, 2019.

[7] M. F. Iqbal, "Prediction of mechanical properties of green concrete incorporating waste foundry sand based on gene expression programming," *Journal of Hazardous Materials*, vol. 384, p. 17, 2020.

[8] A. I. Khan and D. O'Hare, "Intercalation chemistry of layered double hydroxides: recent developments and applications," *Journal of Materials Chemistry*, vol. 12, no. 11, pp. 3191–3198, 2002.

[9] V. R. L. Constantino and T. J. Pinnavaia, "Basic properties of Mg2+1-xAl3+x layered double hydroxides intercalated by carbonate, hydroxide, chloride, and sulfate anions," *Inorganic Chemistry*, vol. 34, no. 4, pp. 883–892, 1995.

[10] X. Fang, "Progress in adsorption-enhanced hydrogenation of CO2 on layered double hydroxide (LDH) derived catalysts," *Journal of Industrial and Engineering Chemistry*, vol. 95, pp. 16–27, 2020.

[11] M. Zubair, M. Daud, G. McKay, F. Shehzad, and M. A. Al-Harthi, "Recent progress in layered double hydroxides

(LDH)-containing hybrids as adsorbents for water remediation," *Applied Clay Science*, vol. 143, pp. 279–292, 2017.

[12] M. Daud, "A review on the recent advances, challenges and future aspect of layered double hydroxides (LDH) Containing hybrids as promising adsorbents for dyes removal," *Journal of Molecular Liquids*, vol. 288, Article ID 110989, 2019.

[13] J. K. E. Tan, P. Balan, and N. Birbilis, "Advances in LDH coatings on Mg alloys for biomedical applications: a corrosion perspective," *Applied Clay Science*, vol. 8, Article ID 105948, 2020.

[14] A. I. Khan, "Intercalation and controlled release of pharmaceutically active compounds from a layered double hydroxide," *Chemical Communications*, vol. 22, p. 2342, 2001.

[15] M. P. Bernardo and C. Ribeiro, "Zn-Al-based layered double hydroxides (LDH) active structures for dental restorative materials," *Journal of Materials Research and Technology*, vol. 8, no. 1, pp. 1250–1257, 2019.

[16] F. Amor, "Development of Zn-Al-Ti mixed oxides-modified cement phases for surface photocatalytic performance," *Case Studies in Construction Materials*, vol. 9, Article ID e00209, 2018.

[17] M. Zhang and E. J. Reardon, "Removal of B, Cr, Mo, and Se from wastewater by incorporation into hydrocalumite and ettringite," *Environmental Science & Technology*, vol. 37, no. 13, pp. 2947–2952, 2003.

[18] I. Muhammad Farjad, "Sustainable utilization of foundry waste: forecasting mechanical properties of foundry sand based concrete using multi-expression programming," *Science of the Total Environment*, vol. 780, Article ID 146524, 2021.

[19] L. Raki, J. J. Beaudoin, and L. Mitchell, "Layered double hydroxide-like materials: nanocomposites for use in concrete," *Cement and Concrete Research*, vol. 34, no. 9, pp. 1717–1724, 2004.

[20] J. Plank, Z. Dai, and P. R. Andres, "Preparation and characterization of new Ca-Al-polycarboxylate layered double hydroxides," *Materials Letters*, vol. 60, no. 29-30, pp. 3614–3617, 2006.

[21] D. G. Costa, A. B. Rocha, W. F. Souza, S. S. X. Chiaro, and A. A. Leitão, "Comparative Structural, thermodynamic and electronic analyses of ZnAlAn− hydrotalcite-like compounds (An−Cl−, F−, Br−, OH−, CO_3^{2-} or NO^{3-}): an ab initio study," *Applied Clay Science*, vol. 56, pp. 16–22, 2012.

[22] Z. Yang, H. Fischer, J. Cerezo, J. M. C. Mol, and R. Polder, "Aminobenzoate modified MgAl hydrotalcites as a novel smart additive of reinforced concrete for anticorrosion applications," *Construction and Building Materials*, vol. 47, pp. 1436–1443, 2013.

[23] L. Wang, "Effects of fineness and content of phosphorus slag on cement hydration, permeability, pore structure and fractal dimension of concrete," *Fractals*, vol. 29, no. 2, 2021.

[24] L. Wang, "The influence of fiber type and length on the cracking resistance, durability and pore structure of face slab concrete," *Construction and Building Materials*, vol. 282, 2021.

[25] Q.-f. Liu, G.-l. Feng, J. Xia, J. Yang, and L.-y. Li, "Ionic transport features in concrete composites containing various shaped aggregates: a numerical study," *Composite Structures*, vol. 183, pp. 371–380, 2018.

[26] O. Kayali, M. S. H. Khan, and M. Sharfuddin Ahmed, "The role of hydrotalcite in chloride binding and corrosion protection in concretes with ground granulated blast furnace slag," *Cement and Concrete Composites*, vol. 34, no. 8, pp. 936–945, 2012.

[27] Y. Tian, C. Dong, G. Wang, X. Cheng, and X. Li, "Zn-Al-NO2 layered double hydroxide as a controlled-release corrosion inhibitor for steel reinforcements," *Materials Letters*, vol. 236, pp. 517–520, 2019.

[28] Z. Y. Qu, Q. L. Yu, and H. J. H. Brouwers, "Relationship between the particle size and dosage of LDHs and concrete resistance against chloride ingress," *Cement and Concrete Research*, vol. 105, pp. 81–90, 2018.

[29] Y. Chen, Z. Shui, W. Chen, and G. Chen, "Chloride binding of synthetic Ca-Al-NO3 LDHs in hardened cement paste," *Construction and Building Materials*, vol. 93, pp. 1051–1058, 2015.

[30] B. Wu, "Study on the affinity sequence between inhibitor ions and chloride ions in Mg Al layer double hydroxides and their effects on corrosion protection for carbon steel," *Applied Clay Science*, vol. 180, Article ID 105181, 2019.

[31] Z. Yang, H. Fischer, and R. Polder, "Synthesis and characterization of modified hydrotalcites and their ion exchange characteristics in chloride-rich simulated concrete pore solution," *Cement and Concrete Composites*, vol. 47, pp. 87–93, 2014.

[32] Z. Yang, R. Polder, J. M. C. Mol, and C. Andrade, "The effect of two types of modified Mg-Al hydrotalcites on reinforcement corrosion in cement mortar," *Cement and Concrete Research*, vol. 100, pp. 186–202, 2017.

[33] L. Cao, J. Guo, J. Tian et al., "Preparation of Ca/Al-Layered Double Hydroxide and the influence of their structure on early strength of cement," *Construction and Building Materials*, vol. 184, pp. 203–214, 2018.

[34] X. Guan, H. Li, S. Luo, X. Liu, and J. Zhang, "Influence of LiAl-layered double hydroxides with 3D micro-nano structures on the properties of calcium sulphoaluminate cement clinker," *Cement and Concrete Composites*, vol. 70, pp. 15–23, 2016.

[35] D. Zou, K. Wang, H. Li, and X. Guan, "Effect of LiAl-layered double hydroxides on hydration of calcium sulfoaluminate cement at low temperature," *Construction and Building Materials*, vol. 223, pp. 910–917, 2019.

[36] P. Duan, W. Chen, J. Ma, and Z. Shui, "Influence of layered double hydroxides on microstructure and carbonation resistance of sulphoaluminate cement concrete," *Construction and Building Materials*, vol. 48, pp. 601–609, 2013.

[37] T. Liu, "Effect of MgO, Mg-Al-NO3 LDH and calcined LDH-CO3 on chloride resistance of alkali activated fly ash and slag blends," *Construction and Building Materials*, vol. 250, Article ID 118865, 2020.

[38] Z. H. Shui, R. Yu, Y. X. Chen, P. Duan, J. T. Ma, and X. P. Wang, "Improvement of concrete carbonation resistance based on a structure modified Layered Double Hydroxides (LDHs): experiments and mechanism analysis," *Construction and Building Materials*, vol. 176, pp. 228–240, 2018.

[39] L. Guo, "Improving sulfate attack resistance of concrete by using calcined Mg-Al-CO3 LDHs: adsorption behavior and mechanism," *Construction and Building Materials*, vol. 232, Article ID 117256, 2020.

[40] L. Lv, J. He, M. Wei, D. Evans, and X. Duan, "Factors influencing the removal of fluoride from aqueous solution by calcined Mg-Al-CO3 layered double hydroxides," *Journal of Hazardous Materials*, vol. 133, no. 1-3, pp. 119–128, 2006.

[41] P. Duan, C. Yan, and W. Zhou, "Effects of calcined layered double hydroxides on carbonation of concrete containing fly ash," *Construction and Building Materials*, vol. 160, pp. 725–732, 2018.

[42] S. Yoon, J. Moon, S. Bae, X. Duan, E. P. Giannelis, and P. M. Monteiro, "Chloride adsorption by calcined layered double hydroxides in hardened Portland cement paste,"

Materials Chemistry and Physics, vol. 145, no. 3, pp. 376–386, 2014.

[43] Y. Chen, R. Yu, X. Wang, J. Chen, and Z. Shui, "Evaluation and optimization of ultra-high performance concrete (UHPC) subjected to harsh ocean environment: towards an application of layered double hydroxides (LDHs)," *Construction and Building Materials*, vol. 177, pp. 51–62, 2018.

[44] Y. Wu, P. Duan, and C. Yan, "Role of layered double hydroxides in setting, hydration degree, microstructure and compressive strength of cement paste," *Applied Clay Science*, vol. 158, pp. 123–131, 2018.

[45] J. Geng, "Chloride binding in cement paste with calcined Mg-Al-CO3 LDH (CLDH) under different conditions," *Construction and Building Materials*, vol. 273, Article ID 121678, 2020.

[46] H. Sasanipour, F. Aslani, and J. Taherinezhad, "Chloride ion permeability improvement of recycled aggregate concrete using pretreated recycled aggregates by silica fume slurry," *Construction and Building Materials*, vol. 270, Article ID 121498, 2020.

[47] Q. Wang, Z. Wu, H. H. Tay et al., "High temperature adsorption of CO2 on Mg-Al hydrotalcite: effect of the charge compensating anions and the synthesis pH," *Catalysis Today*, vol. 164, no. 1, pp. 198–203, 2011.

[48] J. K. Das and B. Pradhan, "Long term effect of corrosion inhibitor and associated cation type of chloride ions on chloride profile of concrete exposed to composite chloride-sulfate environment," *Materials Today: Proceedings*, vol. 32, pp. 803–809, 2020.

[49] W. Zhu, R. François, Q. Fang, and D. Zhang, "Influence of long-term chloride diffusion in concrete and the resulting corrosion of reinforcement on the serviceability of RC beams," *Cement and Concrete Composites*, vol. 71, pp. 144–152, 2016.

[50] M. S. H. Khan, O. Kayali, and U. Troitzsch, "Chloride binding capacity of hydrotalcite and the competition with carbonates in ground granulated blast furnace slag concrete," *Materials and Structures*, vol. 49, no. 11, pp. 4609–4619, 2016.

[51] M. Valipour, M. Shekarchi, and M. Arezoumandi, "Chlorine diffusion resistivity of sustainable green concrete in harsh marine environments," *Journal of Cleaner Production*, vol. 142, pp. 4092–4100, 2017.

[52] P. J. Tikalsky, D. Roy, B. Scheetz, and T. Krize, "Redefining cement characteristics for sulfate-resistant Portland cement," *Cement and Concrete Research*, vol. 32, no. 8, pp. 1239–1246, 2002.

[53] L. Jia and X. Lv, "Study on pore structure before and after calcination of hydrotalcite," *Journal of Mudanjiang Normal University (Natural Science Edition)*, vol. 2, pp. 14-15, 2002.